Quantum Dot Peptide Biosensors for Monitoring Caspase 3 Proteolysis and Calcium Ions

Duane E. Prasuhn,[†] Anne Feltz,[‡] Juan B. Blanco-Canosa,[§] Kimihiro Susumu,[∥] Michael H. Stewart,[∥] Bing C. Mei,[∥] Aleksey V. Yakovlev,[‡] Christina Loukou,[⊥] Jean-Maurice Mallet,[⊥] Martin Oheim,[#] Philip E. Dawson,[§] and Igor L. Medintz[†,*]

[†]Center for Bio/Molecular Science and Engineering, Code 6900, [∥]Optical Sciences Division, Code 5611, U.S. Naval Research Laboratory, 4555 Overlook Ave. S.W., Washington, D.C. 20375, [‡]Institut de Biologie, Ecole Normale Supérieure, IBENS, ENS-CNRS UMR 8197, INSERUM U 1024, 46 rue d'Ulm, 75005 Paris, France, [⊥]Département de Chimie, Ecole Normale Supérieure, ENS-CNRS UMR, 8642, 24 rue Lhomond, Paris, F-75005 France, [#]INSERM, U603; CNRS, UMR8154; Université Paris Descartes, Laboratory of Neurophysiology and New Microscopies, 45 rue des Saints Pères, Paris, F-75006 France, and [§]Departments of Cell Biology and Chemistry, The Scripps Research Institute, La Jolla, California 92037

ABSTRACT The nanoscale size and unique optical properties of semiconductor quantum dots (QDs) have made them attractive as central photoluminescent scaffolds for a variety of biosensing platforms. In this report we functionalize QDs with dye-labeled peptides using two different linkage chemistries to yield Förster resonance energy transfer (FRET)-based sensors capable of monitoring either enzymatic activity or ionic presence. The first sensor targets the proteolytic activity of caspase 3, a key downstream effector of apoptosis. This QD conjugate utilized carbodiimide chemistry to covalently link dye-labeled peptide substrates to the terminal carboxyl groups on the QD's surface hydrophilic ligands in a quantitative manner. Caspase 3 cleaved the peptide substrate and disrupted QD donor-dye acceptor FRET providing signal transduction of enzymatic activity and allowing derivation of relevant Michaelis—Menten kinetic descriptors. The second sensor was designed to monitor Ca^{2+} ions that are ubiquitous in many biological processes. For this sensor, Cu^{+}-catalyzed [3 + 2] azide—alkyne cycloaddition was exploited to attach a recently developed azide-functionalized CalciumRuby-Cl indicator dye to a cognate alkyne group present on the terminus of a modified peptide. The labeled peptide also expressed a polyhistidine sequence, which facilitated its subsequent metal-affinity coordination to the QD surface establishing the final FRET sensing construct. Adding exogenous Ca^{2+} to the sensor solution increased the dyes fluorescence, altering the donor—acceptor emission ratio and manifested a dissociation constant similar to that of the native dye. These results highlight the potential for combining peptides with QDs using different chemistries to create sensors for monitoring chemical compounds and biological processes.

KEYWORDS: quantum dot · nanocrystal · biosensor · protease · calcium · FRET · indicator · caspase 3 · fluorescence · energy transfer · dye

Interest in utilizing nanoparticle materials to create hybrid biological-inorganic sensors and probes continues to grow relatively unabated.[1−11] Among available nanomaterials, colloidal semiconductor nanocrystals or quantum dots (QDs) are an appealing choice due to the unique electrochemical and photophysical properties they provide.[4−6,10,12] From an optical perspective these include broad absorption spectra, size-tunable, narrow-symmetric emissions with high quantum yields, large "effective" Stokes shifts, and robust resistance to both photo- and chemical degradation.[4−6] When interfaced with biological molecules including proteins, peptides, and DNA, the resulting QD-biocomposites have widespread applicability in areas ranging from *in vivo* imaging and diagnostics in biomedicine to environmental monitoring for public health and security.[4−6,11,12] QD sensing constructs have already been prototyped for detecting a myriad of targets such as explosives, toxins, nucleic acids, peptides, drugs, carbohydrates, proteins, and enzymatic processes in both ensemble and single-molecule formats.[4,12−15] The principle impediment to further development of these composite nanomaterials continues to be the lack of efficient chemistries for attaching biologicals to QDs with intimate control over their stoichiometry, orientation, and affinity.[16]

We have focused on developing QD biofunctionalization chemistries to address this need. Primary among the strategies we have exploited is that of polyhistidine (His_n) metal-affinity coordination between the imidazolium functional groups on neighboring histidine residues and the Zn present on the QD-ZnS shell.[17] This self-assembly interaction occurs rapidly, with high affinity ($K_d^{-1} \sim 10^9\ M^{-1}$), and is equally effective when using QDs functionalized with either negatively charged or neutral solubilizing ligands. More importantly, it allows control over the average number of molecules attached per QD (valence) through the molar ratios used and even provides spatial orientation of biomolecules on the QD surface

*Address correspondence to igor.medintz@nrl.navy.mil.

Received for review July 12, 2010 and accepted August 20, 2010.

Published online September 7, 2010. 10.1021/nn1016132

© 2010 American Chemical Society

in many cases.[18,19] Recombinant proteins, synthetic peptides, and chemically modified nucleic acids have all been self-assembled to QDs using this approach to create various sensing systems.[17,20−23] For example, we recently engineered the monomeric red fluorescent protein mCherry to express both a terminal His_6-sequence and an intervening caspase 3 cleavage site to yield self-assembled QD-mCherry Förster resonance energy transfer (FRET) sensors capable of monitoring caspase 3 proteolysis.[15] Further work demonstrated a more modular strategy to QD conjugation by incorporating chemoselective, aniline-catalyzed hydrazone coupling chemistry to append His_6 sequences onto peptides and DNA.[24] When this approach was used, His_6-starter peptides were specifically ligated to proteolytic substrate peptides, an oligoarginine cell-penetrating peptide, and even a DNA probe, allowing the subsequently self-assembled QD constructs to engage in appropriately targeted bioassays. Beyond direct His_n-QD self-assembly, concomitant synthesis has developed a family of polyethylene glycol (PEG)-based QD surface functionalizing ligands or caps that are pH stable and that provide access to carbodiimide (EDC)-based linkages or biotin−avidin chemistry.[25] Other research groups have contributed numerous and quite diverse QD bioconjugation strategies ranging from reactive PEG chemistries to adapting Tsien's CrAsH arsenic−tetracysteine linkage chemistry along with demonstrating monovalent labeling.[26−28]

Although significant progress has been made, it still remains important to expand the QD-bioconjugation chemical "toolbox", especially given the current interest in multimodal or theranostic nanomaterials, that is, composites capable of multiple simultaneous applications such as imaging, sensing, and drug delivery.[3,29−31] Successful engineering of next generation materials will be predicated on access to several different biofunctionalization chemistries capable of being simultaneously implemented. Here we demonstrate two different peptide-based chemistries for creating QD sensors, see Figure 1A. In the first, a dye-labeled peptide sequence is coupled to the terminal carboxyl groups of the hydrophilic ligands present on the QD surface using EDC chemistry. The utility of this approach is highlighted by applying the QD-peptide constructs for FRET-based proteolytic sensing. For the latter chemistry, a His_6-appended peptide sequence is covalently linked to CalciumRuby-Cl, a new synthetic Cu^{2+} sensing indicator dye,[32,33] using the Cu^{+}-catalyzed [3 + 2] azide−alkyne cycloaddition (CuAAC) reaction. The indicator dye-peptide construct was subsequently self-assembled to QDs using metal-affinity coordination, allowing the conjugate to function as a FRET-based Ca^{2+} sensor. Despite the fact that the first QD attachment chemistry is covalent, while the latter is self-assembly driven (noncovalent), the ratio of dye-labeled peptide linked to the QDs in each conjugate could still be tightly controlled, allowing each sensor to be applied quantitatively.

RESULTS AND DISCUSSION

Engineering and Function of the Quantum Dot Sensors. Although two different chemistries are employed here, the engineering and function of both sensor constructs have many common attributes, as highlighted in Figure 1A. These include (1) the initial modular design of the peptides themselves, along with the processes of (2) peptide dye-modification, (3) QD conjugation, and (4) FRET sensing. Each peptide sequence is designed to incorporate several functionalities or modules within their respective sequences to facilitate both the chemistry during sensor assembly along with the desired application. For the caspase 3 sensor, peptide **1** displays four relevant functionalities, as highlighted by the colors in Figure 1A. The C-terminal cysteine provides a unique thiol moiety for site-specific labeling with a dye, the SGDEVDSG sequence is an extended recognition site, and substrate for which caspase 3 has demonstrated augmented affinity,[15] the remaining sequence acts as a short spacer, while the single N-terminal primary amine provides the site for covalent linkage to the QD surface-carboxyl ligands. For the Ca^{2+} sensor, peptide **2** displays a unique terminal alkyne group for chemical coupling to the azido-CaRbCl dye, an intervening chemical linkage introduced as part of the azide modification, a sequence rich in Ala and Aib residues that are intended to form an α-helical spacer while the Gly residues are placed to break the helix, and finally, an N-terminal His_6 for metal affinity-driven self-assembly to the QD surface.

Prior to QD conjugation, each peptide was modified with an appropriate dye to facilitate FRET-based sensing. Peptide **1** was labeled with Texas Red dye using standard maleimide−thiol linkage chemistry.[34] As synthesized, the CaRbCl is functionalized with a unique azido handle, providing access to site-specific, orthogonal CuAAC chemistry while leaving the dyes four-pendant, metal-chelating/sensing carboxyl groups unperturbed; their presence specifically precludes EDC chemistry. Peptide **2** was synthesized with a cognate alkyne group and the peptide-CaRbCl conjugate was formed using standard CuAAC aqueous reaction conditions with $CuSO_4$ and ascorbic acid as described in Materials and Methods. The next step in sensor engineering attached the dye-modified peptides to the QDs. For the caspase 3 sensor, Texas Red-labeled peptide **1** was conjugated to the terminal carboxyl groups present on the polyethylene glycol-appended dihydrolipoic acid (DHLA-PEG) surface ligands using EDC-based amide bond formation, see Figure 1 and Materials and Methods.[25,34] Carefully adjusting concentrations of the peptide during the EDC reactions provided control over the average ratio of dye-labeled peptide **1** acceptor conjugate attached per QD donor (*vide infra*). In contrast, the peptide **2**-CaRbCl conjugate was directly

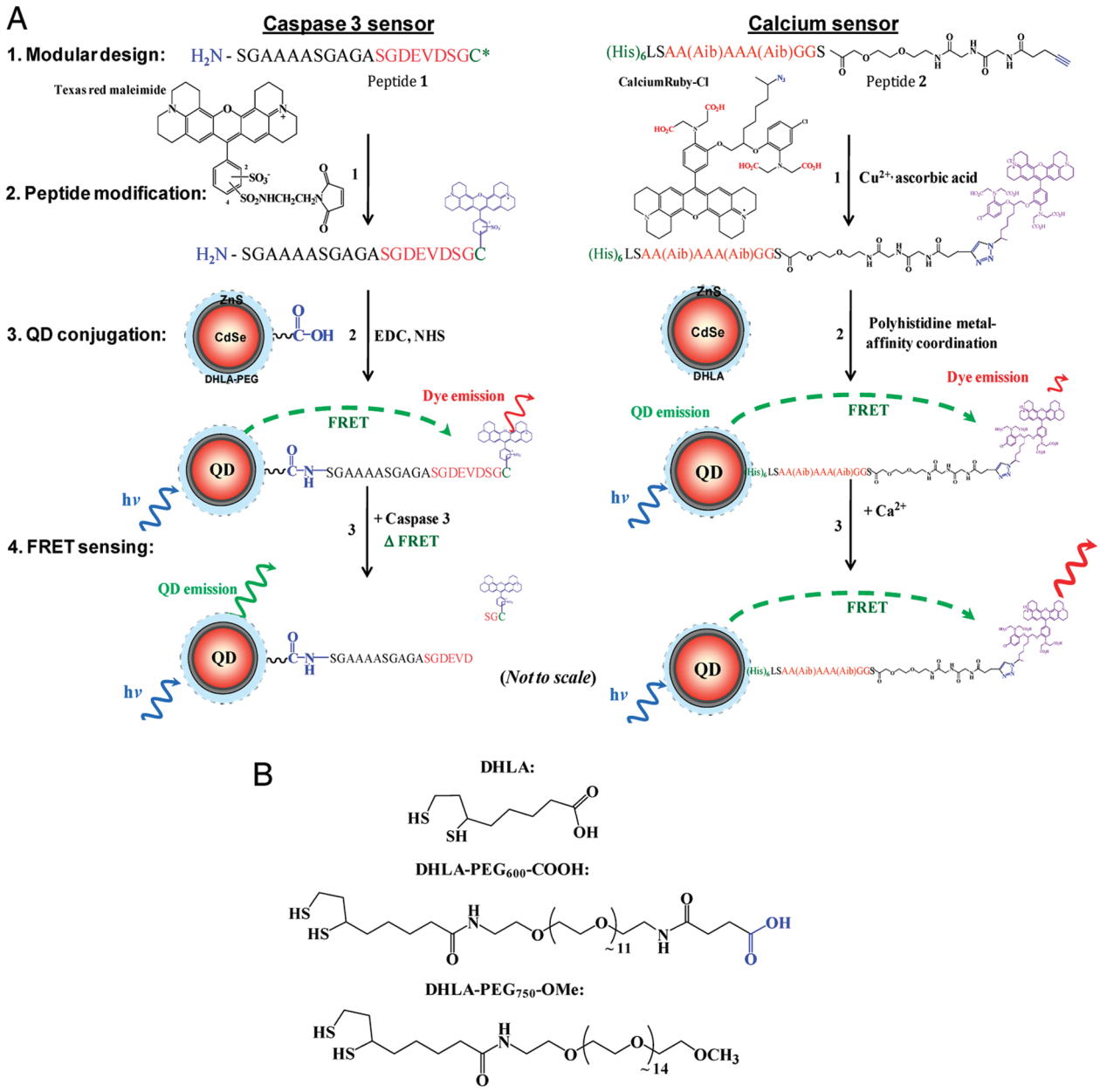

Figure 1. (A) Schematic showing the common design, chemical and sensing elements, including FRET-based biosensors: (1) peptide modularity, (2) peptide labeling, (3) attachment to QDs, and (4) FRET-based sensing for both the caspase 3 proteolytic sensor (left) and Ca^{2+} sensor (right). The 4-pendant carboxyl groups that interact with Ca^{2+} ions are shown in red on the CaRbCl structure. Within the Ca^{2+} sensor peptide sequence, Aib is the synthetic amino acid α-aminoisobutyric acid. Reactive dye structures are shown where appropriate along with the chemical linkages attaching them to the peptides. (B) Chemical structures of the DHLA, DHLA-PEG_{600}-COOH, and DHLA-PEG_{750}-OMe QD surface functionalization ligands used. The carboxyl group targeted by EDC chemistry on the DHLA-PEG_{600}-COOH ligand is highlighted in blue.

mixed with QD solutions for His_6-based self-assembly and final QD-donor to acceptor-dye ratios adjusted through the molar equivalents of each added. Following QD-attachment, both constructs engage in FRET-based or FRET-driven sensing, however, the individual mechanisms that subsequently alter each conjugate's emission and form the basis for signal transduction are quite different. Caspase 3 recognizes and cleaves the DEVD sequence present in peptide **1**, allowing the peptides terminal-three residues with attached dye to diffuse away from close proximity to the QD donor. The rate in which cleavage occurs is proportional to the amount of enzyme and substrate present along with the enzymes specific activity. Rather than depending upon a cleavage event, CaRbCl manifests a ~20-fold increase in quantum yield upon Ca^{2+} binding, making it ideal for detecting changes in this ion concentration. Within the QD-CaRbCl peptide assembly, Ca^{2+} alters the dyes emission properties in a concentration-dependent manner, which in turn alters the ratio of acceptor to donor PL between the QD and CaRbCl. The interested reader is re-

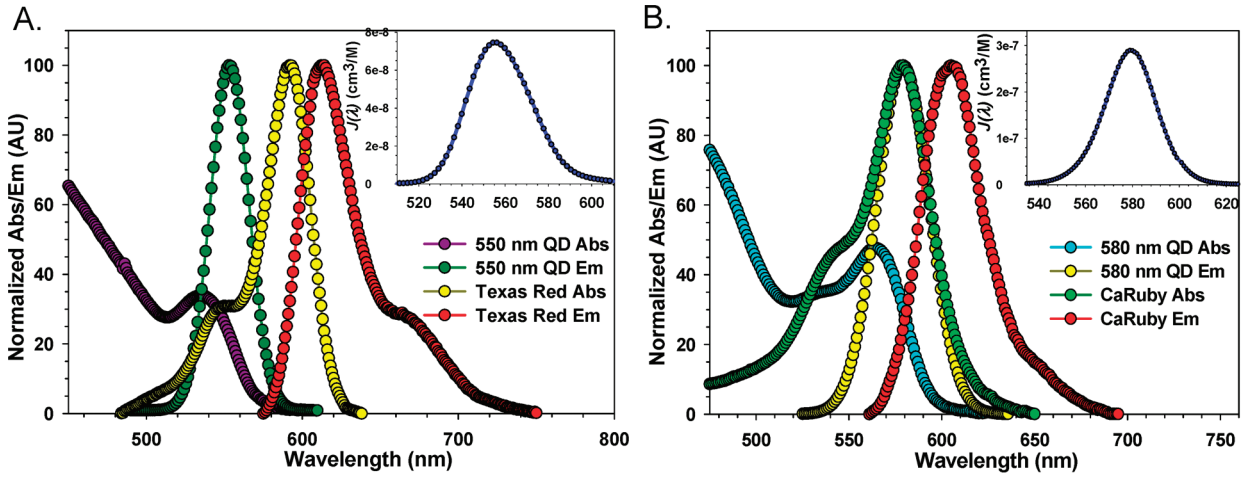

Figure 2. Normalized absorption and emission spectra for the (A) 550 nm emitting QDs-Texas Red and (B) 580 nm emitting QDs-CaRbCl donor−acceptor pairs. The inset in each panel plots the spectral overlap function *J* (λ) *vs* wavelength for each pair.

ferred to ref 32 for a discussion of CaRbCl's original design, synthesis, and characterization.

As shown in Figure 2A, 550 nm emitting QDs were chosen as donors to be paired with the Texas Red acceptor dye. The 550 nm emission overlaps with a significant portion of the Texas Red absorption shoulder and derives a Förster distance (R_0) value of ~46 Å, see Table 1. To optimize FRET with the CaRbCl dye, we utilize a 580 nm emitting QD as it provides excellent overlap with the dye absorption. Indeed, the combination of larger spectral overlap along with the higher acceptor molecular extinction coefficient and similar quantum yield allow for an R_0 value of 56 Å, which is almost 20% better than the 550 nm QD-Texas Red pair. Considering that the QD core/shell radii are estimated to be 28−31 Å, depending upon sample (Table 1), in conjunction with estimates of the peptide lengths in a fully extended confirmation,[18,35] a first approximation suggested that these donor−acceptor pairings would be appropriate for the desired sensing.

Caspase 3 Proteolytic Sensor. Apopain or caspase 3 is an essential downstream effector protease in programmed cell death or apoptosis. Upon activation by upstream initiator caspases, this cysteine protease cleaves substrate proteins containing DEVD target sequences as part of the apoptotic proteolytic cascade.[36] Caspase 3 is of interest in cancer research as its activity has shown to be down-regulated in a variety of breast, ovarian, prostate and gastric tumors.[36] Decreased activity is also a prognostic indicator of chemosensitivity in certain tumors.[37−39] Caspase 3 is also thought to be involved with the neural cell death found in Alzheimer's disease.[40] Developing biosensors capable of monitoring specific activity within both *in vitro* and *in vivo* high-throughput formats continues to be a research priority.

Initial test reaction results showed that a series of QD−peptide conjugates could be constructed over a small range of acceptor ratios (*n*). The superimposed spectra in Figure 3A highlight a representative data set that covers a range of ratios from 0.5 up to 4.3 Texas Red-labeled peptide acceptors/QD in six incremental steps. The spectral separation between donor/acceptor emissions allows data to be directly analyzed from these spectra without requiring subsequent deconvolution. The corresponding QD donor quenching or PL loss, acceptor re-emission or sensitization, FRET efficiency *E*, and *E* corrected for self-assembly heterogeneity are plotted in Figure 3B (see Materials and Methods). FRET efficiency data were corrected because, similar to polyhistidine driven self-assembly to QDs, issues of labeling heterogeneity with concomitant effects on FRET are also applicable in this case.[19] Although not spanning a wide set of acceptor ratios, data show changes in FRET *E* range from 30 to 75%, while the acceptor sensitization increases from ~10 to 35% and derive a donor−acceptor center-to-center separation distance *r* of ~45 Å. Moreover, *E* corrected does not deviate much from initially derived data, indicating no significant heterogeneity effects at the low acceptor ratios used here. As the dye-labeled peptide is attached to the terminal end of the DHLA-PEG_{600}-COOH ligands, its lateral extension directly influences FRET efficiency. Use of a longer PEG derivative when synthesizing the surface ligand would decrease overall FRET *E*. Sparse information is available on the actual number of dithiol ligands that functionalize the surface of CdSe/ZnS QDs.

TABLE 1. Relevant Photophysical Parameters

QD donor λ_{em} (nm)	surface ligand	QD core/shell radius (Å)[b]	acceptor dye	dye $\lambda_{abs}/\lambda_{em}$ (nm)	dye ext. coeff. (M^{-1} cm^{-1})	R_o (Å)	*r* (Å)
550[a]	DHLA-$PEG_{750/600}$ OME/COOH (85:15)	13−14/15	Texas Red	595/615[c]	80,000	46	45
580[a]	DHLA	15−16/15	CaRbCl	579/598[d]	100,000	56	49

[a]Quantum yield of ~20%. [b]Assuming five monolayers of ZnS overcoating.[58,59] [c]Quantum yield of ~25%. [d]Quantum yield of 2.6% for Ca^{2+}-free and 42% for Ca^{2+}-bound.

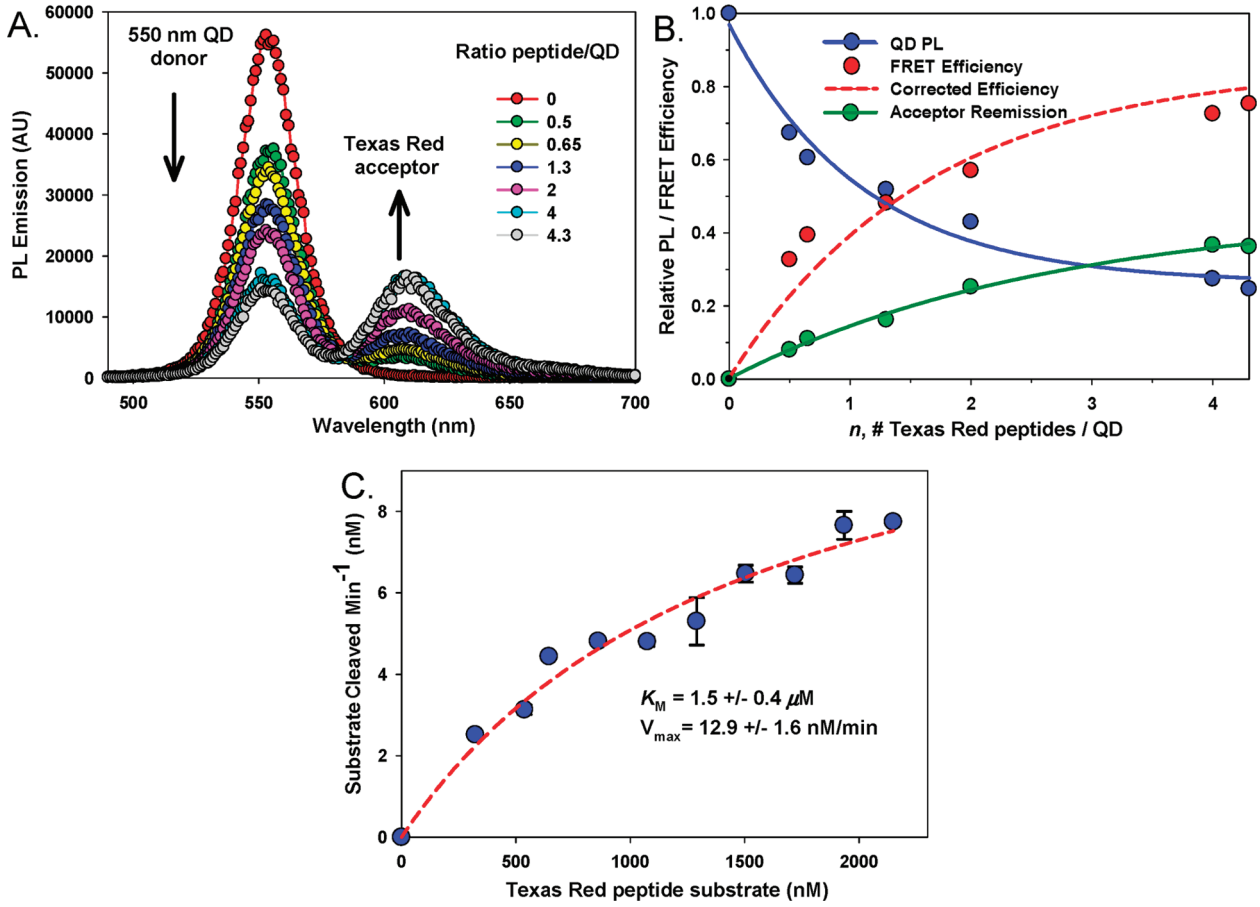

Figure 3. (A) Representative, superimposed spectra collected from 550 nm emitting QD donors surface functionalized with 85:15 DHLA-PEG$_{600}$-COOH/DHLA-PEG$_{750}$-OMe ligands and covalently conjugated to increasing molar ratios of Texas Red-labeled substrate peptide. Samples excited at 350 nm. (B) Plots of corresponding QD PL loss, FRET efficiency *E*, heterogeneity-corrected efficiency, and sensitized Texas Red-acceptor emission calculated from the data in A. (C) Proteolytic assay data from exposing a constant concentration of 550 nm emitting QDs conjugated to 4 Texas Red substrate peptides to a constant concentration of caspase 3 enzyme. Derived K_m and V_{max} values are given. An $R^2 = 0.98$ was obtained for the fitting of the curve.

We have previously estimated a maximum range of ~160−250 ligands,[41] while the Bawendi group has reported average values of 140 ligands for similar QDs.[42] Assuming efficient surface cap exchange and based on the former report, this translates into an estimated minimum of ~21−24 carboxyl groups available on average for the QD samples utilized here, which were functionalized with a mixture containing 15:85 carboxyl/methoxy-terminated ligands. Direct thiol-modification of the surface with acceptor peptide is a possible alternate approach to creating these types of sensors. However, this would involve displacing the solubilizing ligand, which also tends to destabilize the QDs colloidal nature. Furthermore, it is far harder to exert ratiometric control over acceptor valence with the latter approach.

Several criteria are considered when selecting the peptide/acceptor ratio to be utilized as a substrate in assays, and principal among these are significant FRET combined with the potential for a large dynamic change in FRET *E* following proteolysis.[18] As such, we chose to utilize the sample with four peptides/QD as substrate in the assay. Triplicate samples at concentrations ranging from 7.5 to 50 pmols of QD decorated with four peptides each were exposed to 65 units of caspase 3 per reaction, while samples containing no enzyme were used as negative controls. Figure 3C plots the resulting data from the assay following conversion into units of enzymatic velocity (nmol peptidyl substrate cleaved per min). Kinetic analysis derived a K_M of 1.5 ± 0.4 μM, V_{max} of 12.9 ± 1.6 nM min^{-1}, k_{cat} of 0.4 s^{-1} (V_{max}/[Enz$_{total}$] for excess substrate formats), and turnover number k_{cat}/K_M of 2.6 × 10^5 M^{-1} s^{-1}. These values are quite comparable to those previously derived (K_M of 3.0 ± 1.5 μM, V_{max} of 47 ± 30 nM min^{-1}, k_{cat} of 2 s^{-1}, k_{cat}/K_M of 6.7 × 10^5 M^{-1} s^{-1}) with a similar peptidyl substrate assembled on QDs or appended to the fluorescent protein in the QD-mCherry sensor construct.[15,24] The values also reflect the high specific activity of this enzyme. The estimated K_M values are slightly better than the ~11 μM value obtained with a solution-phase peptidyl substrate alone.[43] The parity in sensor performance is also found despite several significant differences in conjugate architecture, including covalent *versus* self-assembly chemistry, use of DHLA *versus* DHLA-PEG surface ligands, and the presence of a dye-labeled

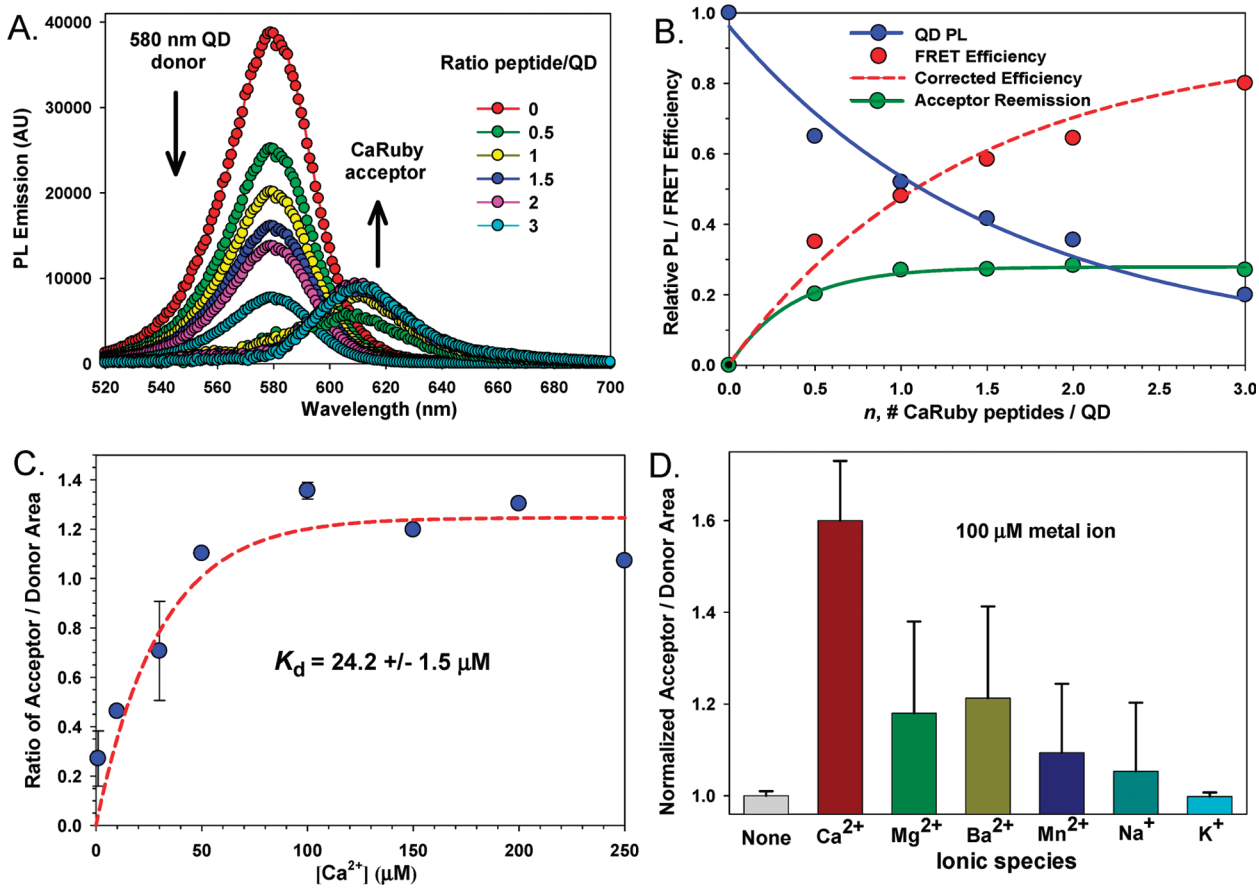

Figure 4. (A) Representative, superimposed, and deconvoluted spectra collected from 580 nm emitting QD donors self-assembled with increasing CaRbCl-acceptor labeled peptides. Samples were excited at 350 nm. (B) Plots of corresponding QD PL loss, FRET efficiency *E*, heterogeneity-corrected efficiency, and CaRbCl-acceptor sensitization from the data in A. (C) Representative data collected from exposing 580 nm QDs self-assembled with ~2 CaRbCl-acceptor labeled peptides to increasing concentrations of Ca^{2+}. The ratio of deconvoluted acceptor/donor PL area are plotted against concentration and used to derive the binding curve and dissociation constant. (D) Normalized acceptor/donor PL area ratios for 580 nm QDs self-assembled with ~2 CaRbCl-acceptor labeled peptides exposed to selected ionic materials. The ratio from the native unexposed sensor was set to an initial value of 1 for comparison purposes.

peptidyl acceptor construct (MW ~ 0.8 kDa) as compared to that of a fluorescent protein (MW ~ 27 kDa).[15] Successful use of QDs functionalized with PEGylated ligands also demonstrates that the QD PEG surface does not sterically prevent protease binding and cleavage of the substrate peptide while attached to the QD. Further, this approach shows that comparable QD-based sensing of caspase 3 can be achieved by coupling accessible peptide sequences and EDC chemistry in contrast to relying on recombinant engineering of a fluorecent protein substrate which also requires maturation and purification prior to self-assembly on a QD.[15] The use of PEG-carbodiimide reactive chemistry recently developed by Snee may be an excellent facilitator for this approach, especially given the high conjugation yields demonstrated with QDs.[26]

Ca^{2+} Sensing Assay. The second messenger Ca^{2+} has numerous biological functions including signal transduction, triggering neurotransmission or muscular contraction, ion channel regulation, blood clotting, skeletal physiology and hormonal signaling to name but a few.[44] Understanding the role of Ca^{2+} in these pathways requires sensitive and specific sensors capable of monitoring rapid changes in Ca^{2+} concentration in a variety of physiological environments.[45] The specific recognition and sensing element within the QD peptide **2** conjugate is the CaRbCl dye acceptor whose pendant carboxyls interact with Ca^{2+} while simultaneously altering the dyes optical properties. We began by similarly characterizing the changes in intra-assembly FRET as an increasing number of CaRbCl-labeled peptide **2** are attached to QDs via metal-affinity self-assembly. The representative data in Figure 4A show spectra where 580 nm emitting QDs made soluble with DHLA were assembled with between 0.5−3 peptides in five incremental steps. Analogous to the results described above, although a small range of acceptor peptide ratios are used, data show changes in FRET *E*, which increases from 35 to 80%, while acceptor sensitization appears to plateau at ~20% in this case (Figure 4B). We attribute the plateau effect noted here for both sensor assemblies to the finite amount of donor energy the QD can provide and not to issues of dye photophysics. A center-to-center QD-donor to dye-acceptor separation distance *r* of ~56 Å is derived from this data, reflecting the slightly larger QD size used in conjunction with the

longer peptide sequence and the presence of connecting spacers on both the peptide and dyes; see schematic in Figure 1A. A relatively good match between FRET *E* and corrected *E* is also seen within this data.

Inspection of this and similar FRET titration data collected using these conjugates led to utilization of a QD construct with a valence of two peptide **2**-CaRbCl per QD for sensing assays. This allows for significant changes in donor/acceptor PL ratios upon Ca^{2+} binding. Stock concentrations of 580 nm QD-peptide **2**-CaRbCl were self-assembled and individual samples aliquoted at concentrations of 0.14 μM QD. Samples were mixed with increasing concentrations of Ca^{2+} ranging from 2 up to 250 μM and resulting changes in emission monitored. As CaRbCl PL increases with increasing Ca^{2+}, we utilized changes in the ratio of CaRbCl acceptor area/QD donor area *versus* [Ca^{2+}] to produce a binding curve and fitting of the assay data derived an apparent dissociation constant K_d of 24.2 ± 1.5 μM with a limit of detection (LOD) of ~2 μM, see Figure 4C. The LOD is defined as a signal-to-noise ratio that is greater than 1 plus 3 times the standard deviation of the blank or zero sample. Exposure of QD only controls to the same concentrations of Ca^{2+} did not significantly alter PL (data not shown). This value is comparable to the K_d of 30.3 ± 2.6 μM previously reported for sensing with the CaRbCl dye alone and indicates that dye-attachment to a peptide and subsequent self-assembly to a QD does not significantly alter its intrinsic Ca^{2+}-sensing properties.[32] It should also be noted that similar K_d values are derived even though all QD conjugate studies were done in deionized water as compared to the buffered solutions originally mentioned in Gaillard *et al.*[32] Those buffers contain nitrilotriacetic acid (NTA), which we have noted can cause demineralization and subsequent quenching of QDs when present free in buffered solution (data not shown). Intracellular and physiological Ca^{2+} concentrations can range from low nM to high μM depending upon activity and context (such as a Ca^{2+} flux) and, thus, sensors with affinities throughout this range are applicable.[45] Assembling the same peptide **2**-CaRbCl onto 580 nm emitting QDs functionalized with a DHLA-PEG_{750}-OMe surface also produced increasing FRET, which tracked peptide valence, however, Ca^{2+} addition did not result in any significant changes in CaRbCl acceptor/QD donor area ratios (data not shown). We speculate that the longer PEGylated ligands on the QD surface may sterically block Ca^{2+} binding to the indicator dye or alternatively its structural rearrangement upon binding. Further experiments with different ligand structures are planned to investigate this issue. We hypothesize that signal transduction in this configuration originates from a Ca^{2+}-dependent change in the radiative rate of CaRbCl dye rather than a change in FRET efficiency. Supporting this, no changes were noted when monitoring peptide **2**-CaRbCl absorption during exposure to the same Ca^{2+} concentrations in the absence of QDs (data not shown). However, the assembly is primarily "driven" by QD FRET sensitization (CaRbCl has only ~10% absorption at the 350 nm used for excitation) and functions in a manner similar to that described for a QD-dye labeled maltose binding protein sugar sensor where allosteric changes in the protein structure upon target binding altered dye emission.[46]

We were also interested in evaluating how the QD-calcium sensor would respond to the presence of other ions in significant concentrations, as this could be predictive of eventual *in vivo* applicability and cross-reactivity. We thus tested the QD sensor construct against Mg^{2+}, Na^{+}, and K^{+} ions, as these are most common to cellular environments, along with Ba^{2+} and Mn^{2+} as control ions with similar valence states. Figure 4D plots the data from exposing sensors at the same valence of two CaRbCl-acceptor labeled peptides per QD to 100 μM of each ion species. This ion concentration was chosen as it represents more than four times the apparent sensor K_d for Ca^{2+}. For direct comparison, the ratios of acceptor/donor area were normalized with the native unexposed sensor ratio set to a value of 1. Calcium ions elicit the greatest change with a ratio of 1.6 ± 0.13 followed by Ba^{2+} and Mg^{2+} with ratios around 1.2 ± 0.2, Mn^{2+} at 1.1 ± 0.15, Na^{+} with 1.05 ± 0.15, and finally K^{+} with a value almost identical to the unexposed sensor. Clearly, the CaRbCl indicator specificity for Ca^{2+} is retained in the QD conjugate assembly. Although Ba^{2+} triggers a strong response, this ion is not normally present biologically at high concentrations, while Na^{+} and K^{+}, which are ubiquitous to biological environments, elicit the smallest sensor responses, respectively, suggesting that sensing may be possible in standard phosphate/saline buffers. Exposing QD controls lacking the peptide **2**-CaRbCl sensing portion to the same ions did not result in any significant gain or loss of PL (data not shown).

Overall, the CuAAC reaction is a rather attractive bioconjugation method due to its intrinsic orthogonality to almost all other functional groups commonly found on biological molecules and has already been successfully implemented in a variety of applications.[47−49] Yet, there are no reports applying this chemistry for direct QD particle functionalization, that is, attachment to pendant QD surface groups *in situ*. Initial experiments revealed that Cu^{2+} significantly and, at times, irreversibly quenched the emission of DHLA or DHLA-PEG-capped QDs utilized, even at concentrations as low as 10 μM (data not shown). The current consensus is that Cu^{2+} and other similar metals interact with the QDs creating surface trap states. Indeed, Chen and Rosenzweig exploited this quenching phenomenon to create QD sensors for a variety of ions, including Ca^{2+} and other species that interact with the QD surface.[50] Thus, for many QD systems, this ligation method is not ideal for direct surface functionalization, but would still be vi-

able as a secondary chemistry independent of the QD, as presented here. Removal of all copper ions from conjugate samples before QD interactions, however, still remains an essential preparatory step. The recent development of copper-free [3 + 2] azide−alkyne cycloaddition chemistry based on strained cyclooctyne groups may represent a possible alternative solution to this issue.[51]

CONCLUSIONS

Here we combine dye-labeled modular peptide sequences with QDs to create composite sensors targeting either enzymatic proteolysis or ionic presence. This work extends the concepts outlined in our previous report where we directly engineered fluorescent proteins or utilized peptide sequences and modular chemistry for assembling QD-based proteolytic substrates along with cellular or DNA hybridization array labels.[15,24,52] We incorporate both standard maleimide labeling along with CuAAC to attach dyes to the peptides during the initial labeling. We also demonstrate both EDC and self-assembly to attach the peptides to either the QD ligands or surface, respectively. Despite these differences, we are still able to control discrete QD acceptor ratio which is the critical element allowing us to convert changes in FRET *E* or emission to quantitative kinetic results. Although both sensors incorporate FRET-based modalities, we show monitoring of quite disparate processes, that is, Ca-binding *versus* enzymatic proteolysis. We also highlight the steps common to each chemistry and suggest that the overall modular approach outlined here may allow for the design of similar sensing assemblies targeting other more diverse processes, including pH.[53]

The use of QD FRET-based signal transduction may provide access to optical properties, which are advantageous in certain sensing scenarios. These include removal of dye-bleaching issues commonly encountered when using direct excitation formats and obviating the need for joint incorporation of an internal standard fluorophore.[53] The ability to excite the sensor at an acceptor's absorption minima, which would significantly reduce its direct excitation component, is important for any FRET-based sensing. Additionally, use of QDs uniquely allows control over the rate of FRET in the assembly by simply altering the ratio of acceptor to donor along with availability of multiphoton excitation of the donor if required and the possibility for multiplex sensing formats.[1,4−6,11] Overall, accumulating progress in engineering QD-based sensors has shown access to similar or even better activities as compared to that of non-nanoparticle designs.[18,53−55] This is important as the next step will be applying these sensors *in vivo* both within cellular and small animal models. It is especially within these environments that the unique optical properties of QDs may truly be exploited to allow the correlation of complex spatiotemporal events. The ability to access several different chemistries that facilitate the assembly of such sensors in a carefully controlled manner will be an important part of their development.

MATERIALS AND METHODS

Peptide Synthesis and Modification. Peptides **1** and **2** were prepared using *in situ* neutralization cycles for Boc-solid-phase-peptide synthesis (Boc-SPPS) on MBHA resin (4-methylbenzhydrylamine) as described;[24] see Figure 1 for sequences. 4-Pentynoic acid was coupled using 4-fold excess over resin employing standard peptide coupling with a 4-fold excess of 0.4 M 2-(6-chloro-1*H*-benzotriazole-1-yl)-1,1,3,3-tetramethylaminium hexafluorophosphate (HCTU) solution and 6-fold excess of *N*,*N*-diispropylethylamine. All peptides were purified by HPLC and sequences confirmed by electrospray ionization mass spectrometry (LC/MS API *I* Plus quadrupole MS, Sciex). Prior to dye-modification reactions, the peptides were desalted on oligonucleotide purification cartridges (OPC, Applied Biosystems), dried in a DNA120 speed-vacuum (ThermoSavant), and stored desiccated as a pellet at −20 °C as described in detail in ref 13. Peptide **1**, containing the SGDEVDSG caspase 3 cleavage site, was labeled with excess of Texas Red C_2-maleimide (Life Technologies) fluorescent dye using standard thiol bioconjugation chemistry.[34] Labeled peptide was purified using mini Ni-NTA agarose resin columns (Qiagen; Valencia, CA), desalted with an OPC, quantitated using Texas Red absorbance (ε_{595} = 80,000 M^{-1} cm^{-1}), dried in the speed-vacuum, and stored at −20 °C.[13] Azide-modified CalciumRuby-Cl (CaRbCl) dye, structure shown in Figure 1, was synthesized as described in reference.[32] Peptide **2** was covalently labeled with the azido-CaRbCl using the Cu^{+}-catalyzed [3 + 2] azide−alkyne cycloaddition (CuAAC) reaction.[49,56,57] Briefly, stock solutions of 10 mM peptide **2** in 10% DMSO/H_2O, 4.9 mM of CaRbCl in 0.1 M Tris buffer pH 8.0, 100 mM of $CuSO_4 \cdot H_2O$ in 0.1 M Tris buffer pH 8.0, and 100 mM of ascorbic acid in 0.1 M Tris buffer pH 8.0 were prepared. Then, reagents were assembled at a final concentration of 1.47 mM CaRbCl, 1 mM peptide **2**, 10 mM Cu^{2+}, and 20 mM ascorbic acid, using 0.1 M Tris buffer pH 8.0 to yield a total volume of 150 uL. The mixture was reacted overnight at room temperature (∼20 h) and peptide **2**-CaRubCl conjugate was purified using mini Ni-NTA agarose resin columns and desalted with an OPC. Peptide **2**-CaRbCl was quantitated using CaRbCl absorbance (ε_{579} = 100,000 M^{-1} cm^{-1}),[32] dried in the speed-vac, and stored at −20 °C until assembled on the QDs. Absorption spectra were collected on an Agilent Technologies 8453 UV−visible spectrophotometer (Santa Clara, CA). All other reagents were purchased from Acros Organics or Sigma-Aldrich and used as received.

Quantum Dots. CdSe/ZnS core/shell QDs with emission maxima centered at 550 or 580 nm were synthesized using standard organometallic chemistry and a mixture of organic ligands including trioctylphosphine/trioctylphosphine oxide (TOP/TOPO) and hexadecylamine.[58,59] The 580 nm emitting QDs were made water-soluble by cap-exchanging with dihydrolipoic acid (DHLA), while the 550 nm emitting QDs were cap-exchanged with a mixture of 85:15 polyethylene glycol(PEG)-appended DHLA ligands that terminated in either a methoxy or a carboxyl group, respectively.[25] PEG with MW ∼600 was utilized for the carboyxlated ligands while PEG with MW ∼750 was used with the methoxy ligands (DHLA-PEG_{600}-COOH/DHLA-PEG_{750}-OMe). See Figure 1B for structures.

Assembling Peptide-Functionalized Quantum Dots. 550 nm emitting QDs solubilized with the carboxy-ligands were covalently linked to Texas Red-labeled peptide **1** through amide bond formation. A total of 1 nmol of QD sample in phosphate buffered saline (137 mM NaCl, 10 mM phosphate, 2.7 mM KCl, pH 7.4, PBS) was activated with 50 μmol of 1-ethyl-3-(3-dimethylaminopropyl)carbodiimide (EDC, Pierce

Biotechnology, Rockford, IL) and 2.5 μmol of *N*-hydroxysulfosuccinimide (sulfo-NHS, Pierce) and then mixed with increasing concentrations of the peptide ranging from equimolar to ~30× molar excess added per reaction. Peptide-labeled QDs were purified post-reaction using PD-10 gel permeation columns and 0.1x PBS buffer (GE Healthcare, Piscataway NJ). 580 nm emitting DHLA QDs were self-assembled with increasing CaRubCl-peptide ratios. For FRET monitoring, peptide **2** was initially resuspended in 10% dimethyl sulfoxide (DMSO)/1× PBS buffer, then mixed with 580 nm emitting QDs at the desired molar ratio of peptide **2**-CaRbCl/QD and incubated for ~30 min at room temperature. Samples of self-assembled QDs were made fresh prior to use while the QD-peptide **1** conjugate were found to be stable at 4 °C for >1 month.

Förster Resonance Energy Transfer Analyses of Quantum Dot-Dye Constructs. Fluorescence spectra were collected on a Tecan Safire Dual Monochromator Multifunction Microtiter Plate Reader (Durham, NC). For FRET studies, 100 μL aliquots of individual QD-conjugate reactions were transferred to polystyrene 96-well microtiter plates with nonbinding surfaces (Corning, Corning, NY) and excited at 350 nm. Individual spectra were deconvoluted using OriginLab (OriginLab Corp., Northampton, MA) or SigmaPlot (Systat Software, San Jose, CA) by comparison to spectra collected from the individual components alone to yield separate QD and dye-acceptor emission profiles for each corresponding peptide/QD ratio where appropriate. FRET efficiency E_n (n = number of dye-acceptors per QD) was determined using:

$$E_n = \frac{(F_D - F_{DA})}{F_D} \quad (1)$$

where F_D and F_{DA} are the fluorescence intensities of the donor in the absence and presence of acceptor(s), respectively.[60] Data from FRET efficiency was analyzed using Förster theory to determine the values for center-to-center (QD-to-dye) separation distance r using:

$$r = R_0(n(1 - E)/E)^{1/6} \quad (2)$$

where R_0 designates the Förster distance corresponding to 50% energy transfer efficiency for a single donor−single acceptor configuration.[60] Eq 2 is applicable to single QD/multi-peptide-dye conjugates as it specifically incorporates the presence of multiple acceptors centro-symmetrically arrayed around the QD donor.[61] To account for the effects of heterogeneity in conjugate acceptor ratios resulting during self-assembly or EDC conjugation, in particular at low ratios with high FRET efficiencies, a Poisson distribution function $p(N,n)$ was used.[19] FRET efficiency E from Eq 2 is now derived as

$$E = \sum_n p(N,n)E(n) \quad \text{and} \quad p(N,n) = N^n \frac{e^{-N}}{n!} \quad (3)$$

where n is the exact numbers of acceptors (valence) for conjugates with a nominal average valence of N.

Caspase 3 Proteolytic Assay. Caspase 3 proteolytic activity was assayed in a manner similar to that described before.[15,18,24] 550 nm emitting QD covalently linked to increasing ratios of Texas Red-labeled peptide **1** served to provide the calibration or standard curves. These were generated using the inverse ratio of the Texas Red peak emission PL (~615 nm) to the QD peak PL (550 nm) for each valence of peptide **1**/QD. Texas Red-labeled peptide **1**-QD substrates in 0.4× PBS pH 8.0 were aliquoted into 0.5 mL microcentrifuge tubes at concentrations ranging from 7.5 to 50 pmols of QD per reaction. Recombinant human caspase 3 enzyme (EC#3.4.22.56, activity ≤5.3×10^6 units/mg, Calbiochem, San Diego, CA) was diluted in the same buffer to a stock concentration of 3.25 units/μL, then 65 units were added to the reactions to bring the QD-peptide substrate up to a final volume of 100 μL. Samples containing no enzyme were used as negative controls. Reactions were incubated for 30 min at 30 °C and 5 μL of a 7.5 mg/mL stock of α-iodoacetamide alkylating agent in 0.4× PBS pH 8.0 was added to halt the reaction. Samples were transferred to a microtiter-well plate and emission spectra collected on the Tecan Safire for analysis. Calibration equations (fits to the standard curve data) were used to correlate the changes in FRET E observed after the reaction into the number of Texas Red-labeled peptide **1** cleaved per QD during the assay as described.[15,18,24] The Michaelis constant K_M and maximal velocity V_{max} were estimated using Michaelis−Menten formalism for excess substrate reactions:[15,18,24,43]

$$V = \frac{d[P]}{dt} = \frac{V_{max}[S]}{K_M + [S]} \quad (4)$$

where $[S]$ is substrate, $[P]$ is product (cleaved peptide), and t is time. The data in Figure 3C were fitted using a one-site saturation ligand binding curve in SigmaPlot, version 9 (Systat Software; San Jose, CA).

Ca^{2+} Sensing Assay. Stock solutions of 1 μM 580 nm emitting DHLA QD in Milli-Q deionized (DI) H_2O, 5 μM peptide **2**-CaRbCl in DI H_2O, and 500 μM $CaCl_2 \cdot 2H_2O$ in DI H_2O were initially prepared. Peptide **2**-CaRbCl was self-assembled to QDs (as described) at a ratio of two conjugates per QD and then supplemented with Ca^{2+} ranging in concentration from 0 to 250 μM following the protocol described in ref 32. After ~30 min incubation, samples were excited at 350 nm, and emission spectra were collected and deconvoluted to yield the individual QD donor and peptide **2**-CaRbCl acceptor emission profiles. Each curve was integrated and the ratio of acceptor area/donor area calculated for each $[Ca^{2+}]$ point to generate a binding curve. Fitting the curve with a Hill function in SigmaPlot derived the apparent dissociation constant (K_d) for this system.[32] A similar procedure was used for assaying $BaCl_2 \cdot 2H_2O$, $MnCl_2 \cdot 4H_2O$, $MgCl_2$, NaCl, and KCl salt effects on the sensor. For comparison purposes, the ratios of acceptor/donor area were normalized with the native unexposed sensor ratio set to a value of 1.

Acknowledgment. The authors thank H. Mattoussi and acknowledge the CB Directorate/Physical S&T Division DTRA/ARO, ONR, NRL, and the NRL-NSI for financial support. D.E.P is supported by an American Society for Engineering Education Fellowship through NRL. A.F., J.-M.M., and M.O. received funding from the French Agence National de la Recherche (ANR PNANO 05-051, ANR P3N 09-044-02). J.B.B.-C acknowledges a Marie Curie IOF.

REFERENCES AND NOTES

1. Algar, W. R.; Krull, U. J. Towards Multi-Colour Strategies for the Detection of Oligonucleotide Hybridization Using Quantum Dots as Energy Donors in Fluorescence Resonance Energy Transfer (FRET). *Anal. Chim. Acta* **2007**, *581*, 193–201.
2. He, J.; VanBrocklin, H. F.; Franc, B. L.; Seo, Y.; Jones, E. F. Nanoprobes for Medical Diagnosis: Current Status of Nanotechnology in Molecular Imaging. *Curr. Nanosci.* **2008**, *4*, 17–29.
3. Louie, A. Multimodality Imaging Probes: Design and Challenges. *Chem. Rev.* **2010**, *110*, 3146–3195.
4. Algar, W. R.; Massey, M.; Krull, U. J. The Application of Quantum Dots, Gold Nanoparticles and Molecular Switches to Optical Nucleic-Acid Diagnostics. *Trac-Trends Anal. Chem.* **2009**, *28*, 292–306.
5. Klostranec, J. M.; Chan, W. C. W. Quantum Dots in Biological and Biomedical Research: Recent Progress and Present Challenges. *Adv. Mater.* **2006**, *18*, 1953–1964.
6. Zhang, F.; Ali, Z.; Amin, F.; Riedinger, A.; Parak, W. J. In Vitro and Intracellular Sensing by Using the Photoluminescence of Quantum Dots. *Anal. Bioanal. Chem.* **2010**, *397*, 935–942.
7. Yue, Z.; Khalid, W.; Zanella, M.; Abbasi, A. Z.; Pfreundt, A.; Rivera Gil, P.; Schubert, K.; Lisdat, F.; Parak, W. J. Evaluation of Quantum Dots Applied as Switchable Layer in a Light-Controlled Electrochemical Sensor. *Anal. Bioanal. Chem.* **2010**, *396*, 1095–1103.
8. De, M.; Ghosh, P. S.; Rotello, V. M. Applications of Nanoparticles in Biology. *Adv. Mater.* **2008**, *20*, 4225–4241.
9. Burda, C.; Chen, X. B.; Narayanan, R.; El-Sayed, M. A.

Chemistry and Properties of Nanocrystals of Different Shapes. *Chem. Rev.* **2005**, *105*, 1025–1102.
10. Guo, S. J.; Dong, S. J. Biomolecule-Nanoparticle Hybrids for Electrochemical Biosensors. *Trac-Trends Anal. Chem.* **2009**, *28*, 96–109.
11. Asefa, T.; Duncan, C. T.; Sharma, K. K. Recent Advances in Nanostructured Chemosensors and Biosensors. *Analyst* **2009**, *134*, 1980–1990.
12. Gill, R.; Zayats, M.; Willner, I. Semiconductor Quantum Dots for Bioanalysis. *Angew. Chem., Int. Ed.* **2008**, *47*, 7602–7625.
13. Sapsford, K. E.; Farrell, D.; Sun, S.; Rasooly, A.; Mattoussi, H.; Medintz, I. L. Monitoring of Enzymatic Proteolysis on a Electroluminescent-CCD Microchip Platform Using Quantum Dot-Peptide Substrates. *Sens. Actuators, B* **2009**, *139*, 13–21.
14. Sapsford, K. E.; Pons, T.; Medintz, I. L.; Mattoussi, H. Biosensing with Luminescent Semiconductor Quantum Dots. *Sensors* **2006**, *6*, 925–953.
15. Boeneman, K.; Mei, B.; Dennis, A.; Bao, G.; Deschamps, J. R.; Mattoussi, H.; Medintz, I. L. Sensing Caspase 3 Activity With Quantum Dot-Fluorescent Protein Assemblies. *J. Am. Chem. Soc.* **2009**, *131*, 3828–3829.
16. Medintz, I. Universal Tools for Biomolecular Attachment to Surfaces. *Nat. Mater.* **2006**, *5*, 842.
17. Sapsford, K. E.; Pons, T.; Medintz, I. L.; Higashiya, S.; Brunel, F. M.; Dawson, P. E.; Mattoussi, H. Kinetics of Metal-Affinity Driven Self-Assembly Between Proteins or Peptides and CdSe-ZnS Quantum Dots. *J. Phys. Chem. C* **2007**, *111*, 11528–11538.
18. Medintz, I. L.; Clapp, A. R.; Brunel, F. M.; Tiefenbrunn, T.; Uyeda, H. T.; Chang, E. L.; Deschamps, J. R.; Dawson, P. E.; Mattoussi, H. Proteolytic Activity Monitored by Fluorescence Resonance Energy Transfer Through Quantum-Dot-Peptide Conjugates. *Nat. Mater.* **2006**, *5*, 581–589.
19. Pons, T.; Medintz, I. L.; Wang, X.; English, D. S.; Mattoussi, H. Solution-Phase Single Quantum Dot Fluorescence Resonant Energy Transfer Sensing. *J. Am. Chem. Soc.* **2006**, *128*, 15324–15331.
20. Medintz, I. L.; Berti, L.; Pons, T.; Grimes, A. F.; English, D. S.; Alessandrini, A.; Facci, P.; Mattoussi, H. A Reactive Peptidic Linker for Self-Assembling Hybrid Quantum Dot-DNA Bioconjugates. *Nano Lett.* **2007**, *7*, 1741–1748.
21. Pons, T.; Medintz, I. L.; Sapsford, K. E.; Higashiya, S.; Grimes, A. F.; English, D. S.; Mattoussi, H. On the Quenching of Semiconductor Quantum Dot Photoluminescence by Proximal Gold Nanoparticles. *Nano Lett.* **2007**, *7*, 3157–3164.
22. Roullier, V.; Clarke, S.; You, C.; Pinaud, F.; Gouzer, G.; Schaible, D.; Marchi-Artzner, V.; Piehler, J.; Dahan, M. High-Affinity Labeling and Tracking of Individual Histidine-Tagged Proteins in Live Cells Using Ni^{2+}-Nitrilotriacetic Acid Quantum Dot Conjugates. *Nano Lett.* **2009**, *9*, 1228–1234.
23. Dif, A.; Boulmedais, F.; Pinot, M.; Roullier, V.; Baudy-Floc'h, M.; Coquelle, F. M.; Clarke, S.; Neveu, P.; Vignaux, F.; Le Borgne, R.; Dahan, M.; Gueroui, Z.; Marchi-Artzner, V. Small and Stable Peptidic PEGylated Quantum Dots to Target Polyhistidine-Tagged Proteins with Controlled Stoichiometry. *J. Am. Chem. Soc.* **2009**, *131*, 14738–14746.
24. Prashun, D. E.; Blanco-Canosa, J. B.; Vora, G. J.; Delehanty, J. B.; Susumu, K.; Mei, B. C.; Dawson, P. E.; Medintz, I. L. Combining Chemoselective Ligation with Polyhistidine-Driven Self-Assembly for the Modular Display of Biomolecules on Quantum Dots. *ACS Nano* **2010**, *4*, 267–278.
25. Mei, B. C.; Susumu, K.; Medintz, I. L.; Mattoussi, H. Polyethylene Glycol-Based Bidentate Ligands to Enhance Quantum Dot and Gold Nanoparticle Stability in Biological Media. *Nat. Protoc.* **2009**, *4*, 412–423.
26. Shen, H.; Jawaid, A. M.; Snee, P. T. Poly(ethylene glycol) Carbodiimide Coupling Reagents for the Biological and Chemical Functionalization of Water-Soluble Nanoparticles. *ACS Nano* **2009**, *3*, 915–923.
27. Howarth, M.; Liu, W. H.; Puthenveetil, S.; Zheng, Y.; Marshall, L. F.; Schmidt, M. M.; Wittrup, K. D.; Bawendi, M. G.; Ting, A. Y. Monovalent, Reduced-Size Quantum Dots for Imaging Receptors on Living Cells. *Nat. Methods* **2008**, *5*, 397–399.
28. Genin, E.; Carion, O.; Mahler, B.; Dubertret, B.; Arhel, N.; Charneau, P.; Doris, E.; Mioskowski, C. CrAsH-Quantum Dot Nanohybrids for Smart Targeting of Proteins. *J. Am. Chem. Soc.* **2008**, *130*, 8596–8957.
29. Delehanty, J. B.; Boeneman, K.; Bradburne, C. E.; Robertson, K.; Medintz, I. L. Quantum Dots: A Powerful Tool for Understanding the Intricacies of Nanoparticle-Mediated Drug Delivery. *Exp. Opin. Drug Delivery* **2009**, *6*, 1091–1112.
30. Portney, N. G.; Ozkan, M. Nano-oncology: Drug Delivery, Imaging, and Sensing. *Anal. Bioanal. Chem.* **2006**, *384*, 620–630.
31. Emerich, D. F.; Thanos, C. G. The Pinpoint Promise of Nanoparticle-Based Drug Delivery and Molecular Diagnosis. *Biomol. Eng.* **2006**, *23*, 171–184.
32. Gaillard, S.; Yakovlev, A.; Luccardini, C.; Oheim, M.; Feltz, A.; Mallet, J.-M. Synthesis and Characterization of a New Red-Emitting Ca^{+2} Indicator, Calcium Ruby. *Org. Lett.* **2007**, *9*, 2629–2632.
33. Luccardini, C.; Yakovlev, A. V.; Pasche, M.; Gaillard, S.; Li, D. D.; Rousseau, F.; Ly, R.; Becherer, U.; Mallet, J. M.; Feltz, A.; Oheim, M. Measuring Mitochondrial and Cytoplasmic Ca^{2+} in EGFP Expressing Cells with a Low-Affinity Calcium Ruby and its Dextran Conjugate. *Cell Calcium* **2009**, *45*, 275–283.
34. Hermanson, G. T. *Bioconjugate Techniques*, 2nd ed.; Academic Press: San Diego, 2008.
35. Medintz, I. L.; Sapsford, K. E.; Clapp, A. R.; Pons, T.; Higashiya, S.; Welch, J. T.; Mattoussi, H. Designer Variable Repeat Length Polypeptides as Scaffolds for Surface Immobilization of Quantum Dots. *J. Phys. Chem. B* **2006**, *110*, 10683–10690.
36. Cohen, G. M. Caspases: The Executioners of Apoptosis. *Biochem. J.* **1997**, *326*, 1–16.
37. Hunter, A. M.; LaCasse, E. C.; Korneluk, R. G. The Inhibitors of Apoptosis (IAPs) as Cancer Targets. *Apoptosis* **2007**, *12*, 1543–1568.
38. Fischer, U.; Schulze-Osthoff, K. Apoptosis-Based Therapies and Drug Targets. *Cell Death Differ.* **2005**, *12*, 942–961.
39. Fischer, U.; Schulze-Osthoff, K. New Approaches and Therapeutics Targeting Apoptosis in Disease. *Pharm. Rev.* **2005**, *57*, 187–215.
40. Louneva, N.; Cohen, J. W.; Han, L. Y.; Talbot, K.; Wilson, R. S.; Bennett, D. A.; Trojanowski, J. Q.; Arnold, S. E. Caspase-3 is Enriched in Postsynaptic Densities and Increased in Alzheimer's Disease. *Am. J. Pathol.* **2008**, *173*, 1488–1495.
41. Prasuhn, D. E.; Deschamps, J. R.; Susumu, K.; Stewart, M. A.; Boeneman, K.; Blanco-Canosa, J. B.; Dawson, P. E.; Medintz, I. L. Polyvalent Display and Packing of Peptides and Proteins on Semiconductor Quantum Dots: Predicted versus Experimental Results. *Small* **2009**, *6*, 555–564.
42. Liu, W.; Howarth, M.; Greytak, A. B.; Zheng, Y.; Nocera, D. G.; Ting, A. Y.; Bawendi, M. G. Compact Biocompatible Quantum Dots Functionalized for Cellular Imaging. *J. Am. Chem. Soc.* **2008**, *130*, 1274–1284.
43. Talanian, R. V.; Quinlan, C.; Trautz, S.; Hackett, M. C.; Mankovich, J. A.; Banach, D.; Ghayur, T.; Brady, K. D.; Wong, W. W. Substrate Specificities of Caspase Family Proteases. *J. Biol. Chem.* **1997**, *272*, 9677–9682.
44. Alberts, B.; Johnson, A.; Lewis, J.; Raff, M.; Roberts, K.; Walter, P. *Molecular Biology of the Cell*, Reference ed.; Garland Science: Oxford, 2008.
45. Takahashi, A.; Camacho, P.; Lechleiter, J. D.; Herman, B. Measurement of Intracellular Calcium. *Physiol. Rev.* **1999**, *79*, 1089–1125.
46. Medintz, I. L.; Clapp, A. R.; Melinger, J. S.; Deschamps, J. R.; Mattoussi, H. A Reagentless Biosensing Assembly Based on Quantum Dot Donor Förster Resonance Energy Transfer. *Adv. Mater.* **2005**, *17*, 2450–2455.

47. Ngo, J. T.; Champion, J. A.; Mahdavi, A.; Tanrikulu, I. C.; Beatty, K. E.; Connor, R. E.; Yoo, T. H.; Dieterich, D. C.; Schuman, E. M.; Tirrell, D. A. Cell-Selective Metabolic Labeling of Proteins. *Nat. Chem. Biol.* **2009**, *5*, 715–717.
48. Sharpless, K. B.; Manetsch, R. In Situ Click Chemistry: A Powerful Means for Lead Discovery. *Expert Opin. Drug Discovery* **2006**, *1*, 525–538.
49. Bruckman, M. A.; Kaur, G.; Lee, L. A.; Xie, F.; Sepulveda, J.; Breitenkamp, R.; Zhang, X.; Joralemon, M.; Russell, T. P.; Emrick, T.; Wang, Q. Surface Modification of Tobacco Mosaic Virus with "Click" Chemistry. *ChemBioChem* **2008**, *9*, 519–523.
50. Chen, Y.; Rosenzweig, Z. Luminescent CdS Quantum Dots as Selective Ion Probes. *Anal. Chem.* **2002**, *74*, 5132–5138.
51. Codelli, J. A.; Baskin, J. M.; Agard, N. J.; Bertozzi, C. R. Second-Generation Difluorinated Cyclooctynes for Copper-Free Click Chemistry. *J. Am. Chem. Soc.* **2008**, *130*, 11486–11493.
52. Boeneman, K.; Delehanty, J. B.; Susumu, K.; Stewart, M. H.; Medintz, I. L. Intracellular Bioconjugation of Targeted Proteins with Semiconductor Quantum Dots. *J. Am. Chem. Soc.* **2010**, *132*, 5975–5977.
53. Snee, P. T.; Somers, R. C.; Nair, G.; Zimmer, J. P.; Bawendi, M. G.; Nocera, D. G. A Ratiometric CdSe/ZnS Nanocrystal pH Sensor. *J. Am. Chem. Soc.* **2006**, *128*, 13320–13321.
54. Zhang, C. Y.; Yeh, H. C.; Kuroki, M. T.; Wang, T. H. Single-Quantum-Dot-Based DNA Nanosensor. *Nat. Mater.* **2005**, *4*, 826–831.
55. Zhang, C. Y.; Johnson, L. W. Quantum-Dot-Based Nanosensor for RRE IIB RNA-Rev Peptide Interaction Assay. *J. Am. Chem. Soc.* **2006**, *128*, 5324–5325.
56. Tornoe, C. W.; Christensen, C.; Meldal, M. Peptidotriazoles on Solid Phase: [1,2,3]-Triazoles by Regiospecific Copper(i)-Catalyzed 1,3-Dipolar Cycloadditions of Terminal Alkynes to Azides. *J. Org. Chem.* **2002**, *67*, 3057–3064.
57. Rostovtsev, V. V.; Green, L. G.; Fokin, V. V.; Sharpless, K. B. A Stepwise Huisgen Cycloaddition Process: Copper(I)-Catalyzed Regioselective "Ligation" of Azides and Terminal Alkynes. *Angew. Chem., Int. Ed.* **2002**, *41*, 2596–2599.
58. Peng, Z. A.; Peng, X. Formation of High-Quality CdTe, CdSe, and CdS Nanocrystals Using CdO as Precursor. *J. Am. Chem. Soc.* **2001**, *123*, 183–184.
59. Dabbousi, B. O.; Rodriguez-Viejo, J.; Mikulec, F. V.; Heine, J. R.; Mattoussi, H.; Ober, R.; Jensen, K. F.; Bawendi, M. G. (CdSe)ZnS Core-Shell Quantum Dots: Synthesis and Optical and Structural Characterization of a Size Series of Highly Luminescent Materials. *J. Phys. Chem. B* **1997**, *101*, 9463–9475.
60. Lakowicz, J. R. *Principles of Fluorescence Spectroscopy*, 3rd ed.; Springer: New York, 2006.
61. Clapp, A. R.; Medintz, I. L.; Mauro, J. M.; Fisher, B. R.; Bawendi, M. G.; Mattoussi, H. Fluorescence Resonance Energy Transfer Between Quantum Dot Donors and Dye-Labeled Protein Acceptors. *J. Am. Chem. Soc.* **2004**, *126*, 301–310.